AD-751 540

TRANSIENT RADIATION EFFECTS ON DETECTORS

W. J. Moore, et al

Naval Research Laboratory
Washington, D. C.

October 1972

NRL Memorandum Report 2519

Transient Radiation Effects on Detectors

W. J. MOORE

Semiconductors Branch
Solid State Division

and

P. L. RADOFF AND B. MOLNAR

Solid State Applications Branch
Solid State Division

October 1972

NAVAL RESEARCH LABORATORY
Washington, D.C.

UNCLASSIFIED
Security Classification

DOCUMENT CONTROL DATA - R & D

(Security classification of title, body of abstract and indexing annotation must be entered when the overall report is classified)

1. ORIGINATING ACTIVITY (Corporate author)
Naval Research Laboratory
Washington, D.C. 20390

2a. REPORT SECURITY CLASSIFICATION
UNCLASSIFIED

2b. GROUP
---

3. REPORT TITLE
TRANSIENT RADIATION EFFECTS ON DETECTORS

4. DESCRIPTIVE NOTES (Type of report and inclusive dates)
An interim report on a continuing NRL problem.

5. AUTHOR(S) (First name, middle initial, last name)
W. J. Moore, P. L. Radoff, and B. Molnar

6. REPORT DATE	7a. TOTAL NO. OF PAGES	7b. NO. OF REFS
October 1972	24	8

8a. CONTRACT OR GRANT NO.	9a. ORIGINATOR'S REPORT NUMBER(S)
NRL Problem E02-05	NRL Memorandum Report 2519
b. PROJECT NO. DNA Task TA026	
c.	9b. OTHER REPORT NO(S) (Any other numbers that may be assigned this report)
d	

10. DISTRIBUTION STATEMENT
Approved for public release; distribution unlimited.

11 SUPPLEMENTARY NOTES	12 SPONSORING MILITARY ACTIVITY
	Defense Nuclear Agency Washington, D. C. 20305

13. ABSTRACT

Experimental and theoretical effects of displacement damage to infrared detectors from high energy neutrons have been studied. Material parameters which can be radiation dependent and which affect detector performance have been identified. Theoretical studies are presented for both photoconductive and photovoltaic detectors. Experimental results for lead sulfide detectors are presented. Degradation of detector performance has been observed for neutron fluences greater than 10^{12} neutrons / cm^2.

1a

DD FORM 1 NOV 68 1473 (PAGE 1)
S/N 0101-807-6801

UNCLASSIFIED
Security Classification

14 KEY WORDS	LINK A		LINK B		LINK C	
	ROLE	WT	ROLE	WT	ROLE	WT
Infrared detector						
Displacement damage						
Radiation damage						
Photoconductive detector						
Photovoltaic detector						
Lead sulfide detector						
Indium antimonide detector						
Indium arsenide detector						
Mercury cadmium telluride detector						

16

CONTENTS

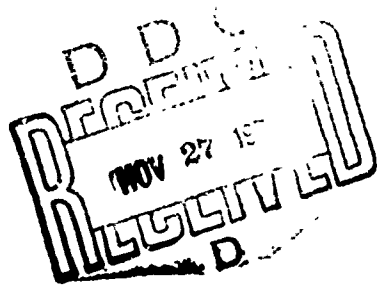

Transient Radiation Effects on Detectors

INTRODUCTION

This report contains the initial results of a study of the long term effects of high energy neutrons on near-infrared detectors. The detectors chosen for this study are lead sulfide, indium antimonide, indium arsenide, and mercury cadmium telluride. All detectors are for use at wavelengths shorter than about six micrometers.

Included in this selection of detectors are one type which operates at room temperature (PbS), three which operate at 78°K, two which are photoconductive (PbS, $Hg_{1-x}Cd_xTe$), and two which are of the photovoltaic type.

Section II of this report contains an analysis of the detection mechanisms and identifies material parameters which influence detector performance and which may be radiation dependent.

The third section contains a description of experiments on lead sulfide detectors. Similar data for InSb, InAs, and $Hg_{1-x}Cd_xTe$ will appear in future reports.

ANALYSIS OF DETECTION MECHANISMS

In order to understand the effects of radiation damage on detectors it is necessary to have a mathematical description of the mechanisms by which the photosignal and the detector noise are produced. It is then possible to identify the material properties which are important in good detectors and which may be radiation dependent.

The detectors chosen for this study include types which are commonly manufactured in the photoconductive form and types which are commonly manufactured in the photovoltaic form. The detection mechanisms are sufficiently different that separate mathematical models are required for each form.

Photoconductive Detectors

Signal Considerations

Photoconductive detectors operate by absorbing quanta of infrared radiation to produce free carriers which increase the detector conductance. This increase in conductance is monitored by suitable

electronic circuits. The detectors chosen for this study are intrinsic detectors, that is, the photon absorption is produced by a mechanism intrinsic to the pure semiconductor and not associated with the impurities in the semiconductor. Impurities do, however, play other important roles in intrinsic detectors, particularly the photovoltaic type.

Semiconductors are characterized by the existence of a forbidden energy gap in which there are no allowed electron states. The lower edge of this gap is the valence band which is normally fully occupied by electrons. Quanta of energy greater than the gap are able to excite electrons from the valence band to the conduction band (the upper limit of the forbidden gap). Both the electron in the conduction band and the unoccupied state (hole) in the valence band can move under the influence of an external electric field. By increasing the number of free charge carriers the infrared radiation increases the detector conductivity which is proportional to the carrier concentration.

Changes in conductivity are monitored using a circuit of the type shown in Fig. 1

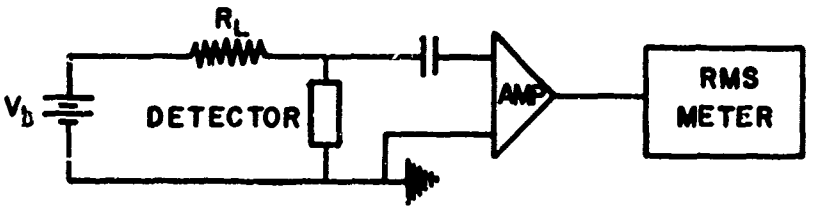

Fig. 1 Typical detector circuitry

The interaction of the detector with its circuitry can be described using the equivalent circuit of Fig. 2

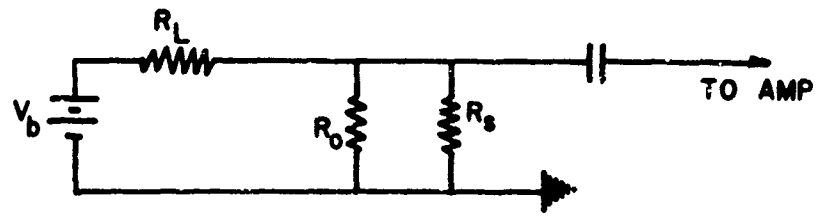

Fig. 2 Detector equivalent circuit

Here V_b is the bias voltage; R_L is the load resistance; R_o is the background resistance, that is, the resistance of the sample when the signal illumination is absent; R_s is the signal resistance which is produced by the photon-generated free carriers. The signal voltage, ΔV_d, resulting from the introduction of the signal resistance, R_s, into the circuit is given by

$$\Delta V_d = V_d \frac{1/R_s}{1/R_o + 1/R_L} \qquad (1)$$

in the small signal approximation, that is, when $R_s \gg R_o$.

Two cases must now be considered. If the load resistance is much larger than the sample resistance this equation reduces to

$$\Delta V_d = V_d \frac{1/R_s}{1/R_o} \quad . \qquad (2)$$

This is the equation for the signal in the constant current condition (the larger load resistor dominates the circuit resistence and therefore the current through the detector is essentially unchanged by the small changes in detector resistance produced by the illumination).

If, on the other hand, the load resistance is small, Eqn. 1 reduces to

$$\Delta V_d = V_d \frac{1/R_s}{1/R_L} \quad . \qquad (3)$$

This is the equation for signal in the constant voltage condition (the voltage across the detector is approximately constant).

In order to determine what information can be obtained from these last two equations we write the background and signal resistances in terms of the microscopic material parameters of the detector:

$$\frac{1}{R_\varepsilon} = \Delta \phi \, \eta_s (\lambda) \, \bar{\tau}_s \, e \, \bar{\mu}_s \, W/L^2 \quad , \qquad (4)$$

where W and L are dimensions of the detector as shown in Fig. 3

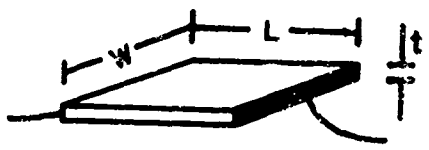

Fig. 3 Detector dimensions

$\Delta\phi$ is the change in the photon flux density due to the signal radiation, $\eta_s (\lambda)$ is the effective quantum efficiency for the creation of electron-hole pairs, and is a function of wavelength, λ , e is the electronic charge and $\bar{\tau}_s$ and $\bar{\mu}_s$ are the effective carrier lifetime and mobility, respectively of the photon-generated carriers. When equal numbers of electrons and holes are produced by the illumination the $\tau\mu$ product is

given by

$$\bar{\tau}_s \bar{\mu}_s = \tau_e \mu_e + \tau_h \mu_h \quad , \tag{5}$$

that is by the sum of the electron and hole $\tau\mu$ products.

In a similar way we can write the background resistance as

$$1/R_o = G \bar{\tau}_o e \bar{\mu}_o 1/L^2 \quad , \tag{6}$$

where G is the total background carrier-generation rate and $\bar{\tau}_o$ and $\bar{\mu}_o$ are the effective lifetimes and mobilities for the background processes.

Some detectors, notably the extrinsic silicon and germanium detectors, have a background generation rate, G, which is proportional to the background photon flux and lifetimes and mobilities which are equal for both the signal and background processes.

In such a situation

$$1/R_o = \phi \bar{\eta}_o (\lambda) WL \bar{\tau}_s e \bar{\mu}_s 1/L \quad . \tag{7}$$

For this situation the signal in the constant current condition becomes

$$\Delta V_d = V_d \frac{\Delta \phi \bar{\eta}_s (\lambda)}{\phi \bar{\eta}_o (\lambda)} \quad . \tag{8}$$

For such detectors the signal is independent of all material parameters except the quantum efficiency.

In order to discuss detectors which do not have this convenient property we can express the lifetimes and mobilities as functions of a parameter α which is a measure of the amount of radiation damage produced. Then

$$\frac{1}{R_s} = \Delta \phi \eta_s (\lambda) WL \bar{\tau}_s (\alpha) e \bar{\mu}_s (\alpha)/L^2 \tag{9}$$

and

$$\frac{1}{R_o} = G \bar{\tau}_o (\alpha) e \bar{\mu}_o (\alpha)/L^2 \quad . \tag{10}$$

The constant current signal for such a case is

$$\Delta V_d = V_d \frac{\Delta\phi\, \eta_s(\lambda)\, W\, \bar{\tau}_s(\alpha)\, \bar{\mu}_s(\alpha)}{G\, \bar{\tau}_o(\alpha)\, \bar{\mu}_o(\alpha)} \quad . \tag{11}$$

If we assume that $\Delta\phi$, W, and G are to first order in α independent of any radiation damage, then we can lump these parameters into a constant, K, and write

$$\Delta V_d = V_d\, K \frac{\bar{\tau}_s(\alpha)\, \bar{\mu}_s(\alpha)}{\bar{\tau}_o(\alpha)\, \bar{\mu}_o(\alpha)}\, \eta_s(\lambda) \quad . \tag{12}$$

The signal, therefore, is changed by radiation damage only when the ratio of the $\tau\mu$ products or the quantum efficiency is changed. If the $\tau\mu$ products for the background processes change in the same way with radiation damage, for instance if they are proportional to α, then the signal is independent of the damage produced. If, however, the signal is experimentally found to be a function of radiation damage we conclude either (1) the $\tau\mu$ products for the signal and background processes are affected differently, or (2) the spectral response $\eta_s(\lambda)$ of the detector is changed.

The signal for the constant voltage condition was given as Eqn. 3

$$\Delta V_d = V_d \frac{1/R_s}{1/R_L} \quad .$$

Here we have only the signal resistance to write in microscopic parameters:

$$\Delta V_d = V_d\, R_L\, \Delta\phi\, \bar{\eta}_s(\lambda) \frac{W}{L^2} \bar{\tau}_s(\alpha)\, e\, \bar{\mu}_s(\alpha) \quad . \tag{13}$$

In this equation it is convenient to introduce the photoconductive gain, g, defined by

$$g(\alpha) = \frac{V_d}{L} \frac{\bar{\tau}_s(\alpha)\, \bar{\mu}_s(\alpha)}{L} \quad , \tag{14}$$

so

$$\Delta V_d = \Delta\phi\, \eta_s(\lambda)\, W\, R_L\, e\, g(\alpha) \quad . \tag{15}$$

Assuming that the dependence of spectral response on radiation

damage is constant to first order, we find that all the radiation effects are in the photoconductive gain term g (ν). Thus, in both constant current and constant voltage conditions, the effect of radiation damage to photoconductive detectors is primarily determined by the change in the $\tau\mu$ product.

Minority Carrier Sweepout

Up to this point we have assumed that radiation damage reduces the $\tau\mu$ product and consequently reduces the signal. Although this is the usual situation it need not hold in all cases. The reason for the possibility of an increase in signal can be understood by considering the effects of the sweepout of minority carriers from the detector. Minority carrier sweepout sets a limit on the achievable gain for intrinsic detectors. The intrinsic signal generation process produces both free holes and free electrons which migrate to opposite electrodes under the influence of the bias field. Assume that the minority carrier mobility is much smaller than the majority carrier mobility. If the bias and lifetimes are sufficiently large the majority carrier will reach its electrode long before the minority carrier is swept out of the crystal. When this happens an additional majority carrier is injected into the crystal from the opposite electrode and continues the conduction process. In this way photoconductive gain in excess of one is possible. An ohmic contact to a semiconductor can be shown to be capable of injecting majority carriers and incapable of injecting minority carriers. Consequently, if the contacts are ohmic, when the minority carrier reaches the electrode no additional minority carriers can be injected. The majority carrier then either recombines to preserve charge neutrally or is swept out, and the conduction process stops. This sweepout of majority carriers places a limit on the photoconductive gain.

Minority carrier sweepout can be delayed with a resulting increase in further photoconductive gain by introducing minority carrier traps which reduce the effective minority carrier mobility. Radiation effects which produce minority carrier traps can therefore increase the minority carrier sweepout time and thereby increase the photoconductive gain and enhance the photosignal.

Noise Considerations[1]

Noise in photoconductive detectors can be classified into three types: (1) generation - recombination noise, (2) Johnson noise, and (3) "1/f" noise.

Generation - recombination noise is a result of the statistical uncertainty in the times of the generation and recombination events. The frequency spectrum of the fluctuations in the concentration of background, non-photon-induced carriers is typically given by

$$\Delta N(\omega) = 2 G^{\frac{1}{2}} \bar{\tau}_o (1 + \omega^2 \bar{\tau}_o^2)^{-\frac{1}{2}} \quad . \tag{16}$$

Treating the concentration fluctuation as a signal, we can substitute for $1/R_s$ the following:

$$1/R_s \rightarrow \Delta N(\omega)\, e\, \mu\, \frac{1}{L^2} \quad .$$

The resulting noise is given by:

$$\text{Constant I:} \quad \Delta V_{dn}(\omega) = V_d \frac{2G^{\frac{1}{2}} \bar{\tau}_o e \bar{\mu}_o \frac{1}{L^2}}{1/R_o (1 + \omega^2 \bar{\tau}_o^2)^{\frac{1}{2}}} \quad . \tag{17}$$

$$\text{Constant V:} \quad \Delta V_{dn}(\omega) = V_d \frac{2G^{\frac{1}{2}} \bar{\tau}_o e \bar{\mu}_o L^{\frac{1}{2}}}{1/R_L (1 + \omega^2 \bar{\tau}_o^2)^{\frac{1}{2}}} \quad . \tag{18}$$

A similar calculation must be made for the photon-generated carriers using the proper expression for generation of hole-electron pairs. This gives

$$\text{Constant I:} \quad \Delta V_{dn}(\omega) = V_d \frac{2(\phi W L \eta_s)^{\frac{1}{2}} \bar{\tau}_s e \bar{\mu}_s \frac{1}{L^2}}{1/R_L (1 + \omega^2 \bar{\tau}_s^2)^{\frac{1}{2}}} \tag{19}$$

$$\text{Constant V:} \quad \Delta V_{dn}(\omega) = V_d \frac{2(\phi W L \eta_s)^{\frac{1}{2}} \bar{\tau}_s e \bar{\mu}_s \frac{1}{L^2}}{1/R_L (1 + \omega^2 \bar{\tau}_s^2)^{\frac{1}{2}}} \tag{20}$$

The total noise from these two generation recombination processes (i.e. signal and background processes) is equal to the sum of these noises added in quadrature, that is, the square root of the sum of the squares of the two processes.

Johnson noise arises from thermal motion of the free carriers. The Johnson noise voltage from a device with resistance R at absolute temperature T measured with a noise bandwidth Δf is given by

$$\Delta V_J = [4k T R \Delta f]^{\frac{1}{2}} \quad . \tag{21}$$

If the detector and its load resistor are not at the same

temperature the expression is more complex. In general, for a set of resistors of resistance R_i at temperature T_i the Johnson noise is

$$\Delta V_J = \left[\prod_i R_i\right]^{\frac{1}{2}} \left[4k\,\Delta f \sum_i T_i R_i\right]^{\frac{1}{2}} / \sum_i R_i \quad . \tag{22}$$

The magnitude of the Johnson noise can be made small by cooling the detector and by minimizing its resistance. "1/f" noise processes are not easily written in analytic form. The current and frequency dependence of the noise voltage is usually of the form

$$\Delta V_f = \Delta f\, C\, I f^{-\frac{1}{2}} \quad , \tag{23}$$

where Δf is the noise bandwidth. The terminology "1/f" refers to the frequency dependence of the noise power. The magnitude of the 1/f noise can be a function of the quality of the electrical contacts to the detector, the surface preparation, and the care with which the sample is handled. Since 1/f noise cannot easily be treated analytically and since most detectors are, if possible, operated at sufficiently high frequencies to avoid this noise we shall assume in the following analysis that it is negligibly small.

Signal to Noise Ratios

As is indicated above the noise contributions of primary concern, if the effects of radiation damage are to be analyzed, is the Johnson noise. Accordingly, the signal-to-Johnson noise ratio should be minimized and, to the extent possible, made independent of the amount of radiation damage produced. For constant - current operation the signal is given by Eqn.(11) and the Johnson noise by Eqn. (21). The single - to - noise ratio is then:

$$\frac{S}{N} = \frac{V_d\, \Delta\phi\, n_s\, W\, \bar{\tau}_s(\nu)\, \bar{\mu}_s(\alpha)}{G\, \bar{\tau}_o(\alpha)\, \bar{\mu}_o(\nu) \sqrt{4k\, T\, \Delta f}\, G^{\frac{1}{2}}\, \bar{\tau}_o^{\frac{1}{2}}\, \bar{\mu}_o^{\frac{1}{2}}\, e^{\frac{1}{2}}\, L} \quad . \tag{24}$$

The radiation dependence is contained in the $\tau\mu$ terms and we can write

$$\frac{S}{N} = K\, \frac{\bar{\tau}_s(\nu)\, \bar{\mu}_s(\nu)}{\bar{\tau}_o^{\frac{1}{2}}(\alpha)\, \bar{\mu}_o^{\frac{1}{2}}(\nu)} \quad . \tag{25}$$

For constant voltage operation we use the expressions for the signal given by Eqn. (15) and for the noise by Eqn. (21). The resistance is that of the load resistor, R_L.

$$\frac{S}{N} = \frac{\Delta\phi\, \eta_s\, W\, L\, R_L^{\frac{1}{2}}\, e\, g\,(\alpha)}{\sqrt{4k\, T\, \Delta f}} \quad . \tag{26}$$

The radiation dependence is in the gain factor exclusively. Therefore any change in the signal - to - noise ratio is due to a change in photoconductive gain.

For situations in which the signal and background time constants and mobilities have the same dependence on α the constant current mode of operation gives a signal - to - noise ratio which varies as $\tau^{\frac{1}{2}}\, \mu^{\frac{1}{2}}$, whereas that for the constant voltage mode varies as $\tau\mu$. Consequently, constant current mode operation is more radiation resistant for this situation.

Photovoltaic Detectors

Signal Considerations[2]

Photovoltaic detectors operate through the creation by incident photons of free electron-hole pairs, as is also the case for photoconductive detectors. Photovoltaic detectors, however, differ from the photoconductive types in the way in which the photon-generated free carriers interact with the detector and the measuring circuit. These differences provide the photovoltaic detector with several advantages.

A photovoltaic detector consists of a junction which can be illiminated and a pair of electrical contacts. In practice detectors are usually made using a "mesa" structure as shown in Fig. 4

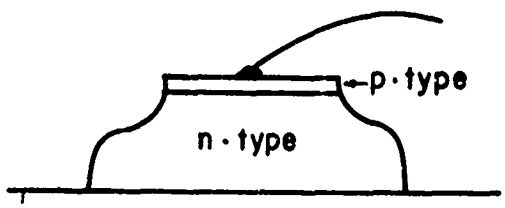

Fig. 4 Typical photovoltaic detector construction

The structure shown in Fig. 4 consists of a p-type layer a few microns thick on an n-type base material (n-on p-structures can also be made). Radiation to be detected falls on the surface of the thin p-type layer. Free electrons and holes are formed within the material near the top surface. If the absorption coefficient is small some carriers can be produced in the junction region or in the n-type base layer. These carriers diffuse toward the junction. Analysis of the electric field configuration in a p-n junction shows that only the minority carriers

which reach the junction from either side are swept out by the field at the junction to produce a flow of current in the external circuit. The total current flowing through the diode is made up of photon-generated currents, thermally generated currents, the ideal diode current given by the Schockley Eqn. and any currents due to leakage across the junction region. In order to calculate the current and noise to be expected from a typical photovoltaic detector we can assume that the detector is cooled sufficiently to cause thermally generated currents to be negligible. The contribution to the diode current from the photon-generated carriers is given by

$$I_{pc} = -A \int_0^{\lambda} \eta(\lambda)\, \phi(\lambda)\, d\lambda \quad , \tag{27}$$

where, as before, e is the electron charge, $\eta(\lambda)$ is the quantum efficiency, $\phi(\lambda)$ is the photon flux density, and A is the diode area. The quantum efficiency $\eta(\lambda)$ is to be understood to represent the probability that a photon incident on the detector surface will produce a hole-electron pair and that the minority carrier so produced will diffuse to the junction region and be swept out. $\eta(\lambda)$, then, will be a function of the photon absorption coefficient, minority carrier diffusion length, and the probability of sweepout.

An ideal diode will carry a current whose value is given by the Schockley Eqn.

$$I_d = I_s \left(e^{eV/\beta k T} - 1\right) . \tag{28}$$

V is the potential across the diode, T is the diode temperature, β is a factor between about one and four, and I_s is the reverse saturation current which is given by

$$I_s = Ae \left[\frac{D_p P_{no}}{L_p} + \frac{D_n N_{po}}{L_n} \right] . \tag{29}$$

Here A is the diode area, D_p and D_n are the hole and electron diffusion coefficients, L_p and L_n are the hole and electron diffusion lengths, P_{no} is the equilibrium concentration of holes in the n-type side, and N_{po} is the equilibrium concentration of electrons on the p-type side.

Any stray conductance G_1 shunting the junction (such as surface leakage) will contribute a current I_1 given by

$$I_1 = G_1 V \quad . \tag{30}$$

The total current across the junction then is

$$I = I_s \left(e^{eV/\beta k T} - 1\right) - e A \phi + G_l V \quad . \tag{31}$$

Modulation of the photon flux will produce a signal given by

$$\Delta I = \frac{dI}{d\phi} \Delta\phi = \left[-eA + I_s \frac{e}{\beta kT} e^{eV/\beta kT} \frac{dV}{d\phi} + G_l \frac{dV}{d\phi}\right] \Delta\phi \quad . \tag{32}$$

Since $\frac{dV}{d\phi}$ is positive, the signal current is out of phase with the other components of this equation and it is therefore desirable to operate with an electrical circuit which will insure that

$$(1)\ \frac{dV}{d\phi} \approx 0 \text{ and } (2)\ V \leq 0 \ .$$

We will see below that similar conditions provide minimum detector noise. In practice, although it is impossible to satisfy these conditions exactly they can be approximately fulfilled: either the detector can be operated into a very low resistance circuit (real or synthesized) or by means of a bias circuit the average value of V can be set to zero.

Noise Considerations[3]

Noise in photovoltaic detectors is primarily (1) generation-recombination noise, (2) shot noise, (3) Johnson noise in the leakage current, and (4) 1/f noise. Generation - recombination noise can be written as shot noise in the photon generated current and so combined with the ideal diode current. The total shot noise is then

$$I_{ns}^2 = \Delta f\ 2\ e \left[I_{pc} + \frac{I_s}{\beta} \left(e^{eV/\beta k T} + 1\right)\right] \quad , \tag{33}$$

where Δf is the noise bandwidth and I_{pc} is the photon generated current.

The Johnson noise in the leakage current is given by (see Eqn. 21)

$$I_{ng}^2 = \Delta f\ 4k\ t\ G_l \quad . \tag{34}$$

As was the case for photoconductive detectors (Eqn. 23) the noise can be written as

$$I_{1/f\ n}^2 = \Delta f\ C^2\ I^2\ f^{-1} \quad . \tag{35}$$

Combining these equations, the total noise current is

$$I_n^2 = 2\,e\,\Delta f\,[\,I_{pc} + \frac{I_s}{\beta}\,(e^{eV/\beta\,k\,T} + 1)] + \Delta f\,4k\,T\,G_l$$

$$+ \Delta f\,C^2 I^2\,f^{-1} \quad , \qquad (36)$$

In order to minimize the noise it is necessary to minimize the diode voltage and current and the leakage conductance.

It is possible to write the signal - to - noise ratio as was done for the photovoltaic case, but this does not lead to analytical simplification. Consideration of both signal and noise indicates that operation near V = 0 is desirable. Experimentally the V = 0 condition is produced either by applying a slight reverse bias to offset the bias produced by the background radiation, or by using an operational amplifier to synthesize a low input impedance current-sensitive amplifier; the former method was used in our experiments.

The radiation-dependent parameters for photovoltaic detectors are the quantum efficiency $\eta\,(\lambda)$, the reverse saturation current I_s, the shunt conductance G_l, and, possibly, the parameter β. $\eta\,(\lambda)$ and I_s are radiation-dependent as a result of radiation-induced variations in the minority carrier diffusion lengths. The leakage conductance, G_l, may be radiation-dependent as a result of radiation-induced surface changes.

GENERAL EXPERIMENTAL CONDITIONS

Determination of Detector Figures of Merit

The determination of the noise equivalent power (NEP) and the black body detectivity (D^*_{bb}) for both PbS and InSb detectors was carried out using equipment shown schematically in Fig. 5

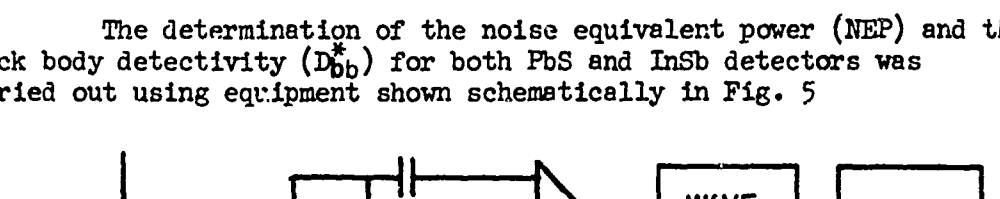

Fig. 5 Block diagram of detector evaluation apparatus

Radiation from a 500°K black body[4] is chopped by a variable speed chopper (2 Hz to 5 kHz)[15] before falling on the detector. The photosignal and noise are amplified by a low noise preamplifier[6] and the rms voltage is determined by a wave analyzer with a 1 Hz band-

width (7). For greater accuracy in determining the noise level the rms noise voltage was displayed on a strip chart recorder and averaged over several minutes. In this way the signal (S) and noise (N) were measured as a function of current, chopping frequency, and neutron fluence.

From these measurements the black body detectivity was obtained from the following relation:

$$D^*_{bb} = \frac{S}{N} \frac{1}{\Delta P_{bb}} A^{\frac{1}{2}}, \qquad (37)$$

where ΔP_{bb} is the rms value of the Fourier component of the chopped radiant power at the chopping frequency.

Neutron Sources

Two principal neutron sources were used: a commercially available neutron generator and the NRL cyclotron.

The commercial source makes use of a deuterium-tritium reaction produced by bombarding a tritiated titanium target with 180 kev deuterons. The reaction is:

$$H^2 + H^3 \rightarrow He^4 + n^1 + 17.6 \text{ MeV}. \qquad (38)$$

This source is capable of producing a usable flux of about 1.6×10^{10} neutrons sec^{-1} $steradian^{-1}$ whose energy distribution is sharply peaked at 14.2 MeV. Irradiations to a total fluence of 9.2×10^{12} n cm^{-2} have been made using this source.

Neutrons are produced in the NRL cyclotron facility when a beryllium target is bombarded with 35 MeV deuterons. A flux of 5×10^{12} n sec^{-1} $ster^{-1}$ is available. The energy distribution, as determined from time-of-flight measurements, is a broad peak centered at about 16 MeV with only a small number of neutrons with energies less than 1 MeV or greater than 30 MeV. See Fig. 6. Fig. 7 shows the angular distribution of neutrons near the forward direction. Gamma rays account for only 5% of the total emitted energy. Since the cyclotron source is far more intense than the deuterium-tritium source, the former was used to produce fluences up to 10^{14} n cm^{-2}.

Overlap of data between the two sources indicates that both neutron sources are about equally effective in causing damage to PbS detectors. Both sources have the highly advantageous property of being virtually free of other types of unwanted radiations such as γ rays.

RESULTS FOR LEAD SULFIDE DETECTORS

Measurements were performed on eleven "Infratron" PbS photoconductors procured from Infrared Industries, Inc., Waltham, Mass.,

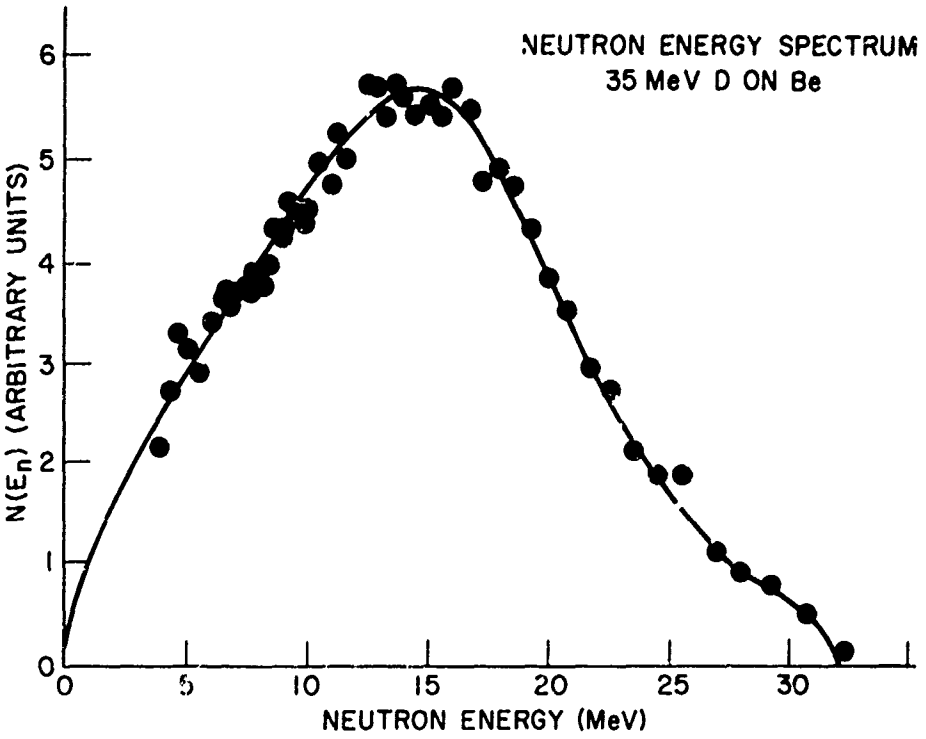

Fig. 6 - Energy distribution of neutrons from NRL cyclotron facility.

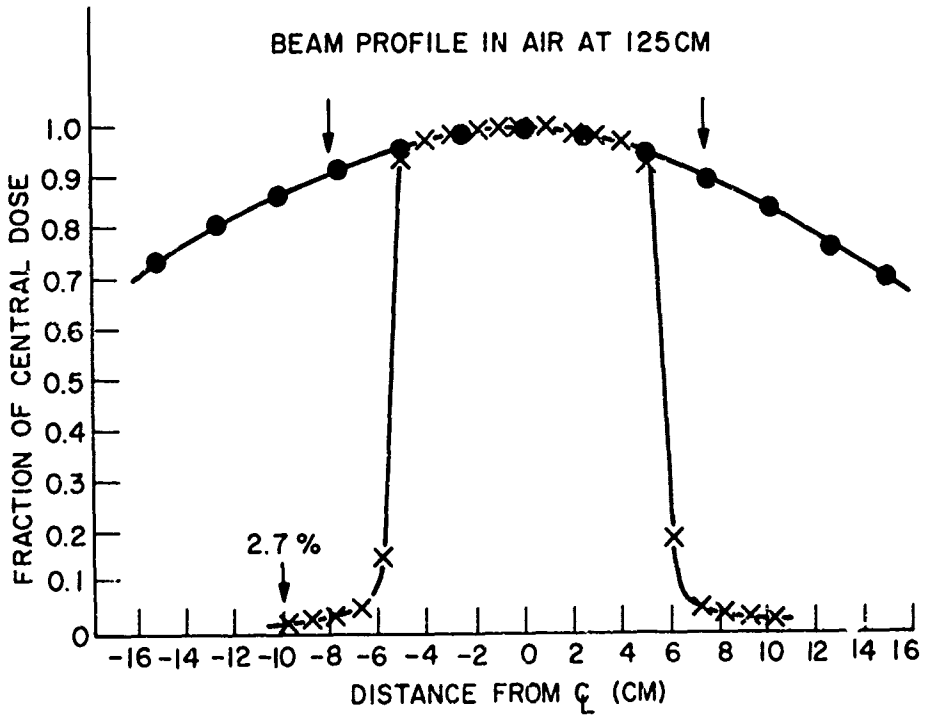

Fig. 7 - Angular distribution of neutrons from NRL cyclotron facility. The profile indicated by x is obtained when a 10 × 10 cm collimator is used. The filled circles indicate the profile of the uncollimated beam used for all of the present measurements.

which had nominal room temperature detectivities (D^*_{bb}) of about $7X10^8$ $cmHz^{\frac{1}{2}}$ $watt^{-1}$. The construction of these detectors is shown in Fig. 8

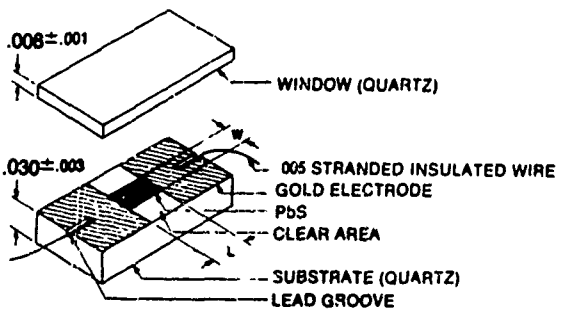

Fig. 8 Lead sulfide detector construction

The sensitive area was 20 mils square for all detectors.

The detectors were irradiated at room temperature and measured after a delay of from several hours to a day. The damage observed is therefore relatively permanent.

In Fig. 9 the frequency dependence of signal and noise for a typical PbS detector in the constant current mode is plotted both before and after irradiation by 10^{13} n cm^{-2}. Both signal and noise decreased after irradiation. The flat (or white) region extending from about 40 Hz to about 200Hz makes it appear that generation-recombination noise is dominant in that region. But as we will later see this is not the case.

The current dependence of signal and noise in the same detector is shown in Fig.10 at a frequency of 100 Hz (which lies well within the white noise region). Again both signal and noise fall after irradiation by 10^{13} n/cm^2.

Fig. 11 shows the radiation dependence of signal, noise, and S/N for neutron fluences up to 10^{14} / cm^2 in the constant mode. (In the constant voltage mode these quantities exhibit qualitively the same behavior.) The curves are composites of several detectors exposed to neutrons from both sources. While the signal shows a monotonic decrease with fluence, the noise exhibits a maximum (and, therefore, S/N a minimum) near 2 X 10^{13} n/cm^2. The threshold fluence for observation of damage is about 2 X 10^{12} n/cm^2.

The maximum signal-to-noise ratio varies considerably from sample to sample. The largest signal-to-noise ratio measured (corresponding to the largest detectivity) was found in sample No. 11 at a chopping frequency of 100 Hz (within the G.R. noise region). The detectivity was D^*_{bb} (500°K, 100, 1) = 7.2 X 10^8 cm $Hz^{\frac{1}{2}}$ $watts^{-1}$. In order to convert D^*_{bb} to $D^*_{\lambda max}$ we can use a conversion factor which is typically about 100 for PbS at 300°K. This results in $D^*_{\lambda max}$ = 7.2 X

10^{10} cm $Hz^{\frac{1}{2}}$ $watts^{-1}$, which is within the range specified by the manufacturer. The detector resistance was essentially unchanged during irradiation.

CONCLUSIONS

Long term effects (of the order of 24 hours and longer) of high energy neutrons on lead sulfide infrared detectors have been observed. Degradation of detector performance was observed for a fluence in excess of about 2 X 10^{12} neutrons cm^{-2}. This result contrasts with earlier studies using thermal neutrons from a reactor[8] in which degradation appeared only after exposure to greater than 10^{14} neutrons cm^{-2}. These results indicate that the thermal neutrons used in the earlier study were about two orders of magnitude less effective than 14 MeV neutrons in producing damage in lead sulfide.

The effects to be expected from bombardment with somewhat lower energy neutrons can be predicted using the 14 MeV damage data and approximate scaling factors.

Annealing studies on these detectors have not been conducted, but future measurements will determine the effects of storage at room temperature over a period of several months. Irradiation and evaluation of photovoltaic indium antimonide and indium arsenide detectors are underway. The results of these studies will appear in a future report.

ACKNOWLEDGMENTS

We are grateful to Richard Theus for use of the cyclotron source and to Al Nash for the operation of the deuterium-tritium source

REFERENCES

1. P.W. Kruse, L.D. McGlauchlin, R.B. McQuistan, Elements of Infrared Technology, John Wiley & Sons, Inc. (New York, 1962).

2. G.R. Pruett and R.L. Petritz, Proc. IRE 47, 1524 (1959).

3. A. Van der Ziel, Noise: Sources, Characterization and Measurement, Prentice-Hall, Inc. (Englewood Cliffs, New Jersey, 1970.)

4. Infrared Industries Model No. 463.

5. Princeton Applied Research Model No. 222.

6. Princeton Applied Research Model No. 113.

7. Quan-tek Model No. 304-R.

8. R.R. Billups and W.L. Gardner, Infrared Phys. 1, 199 (1961).

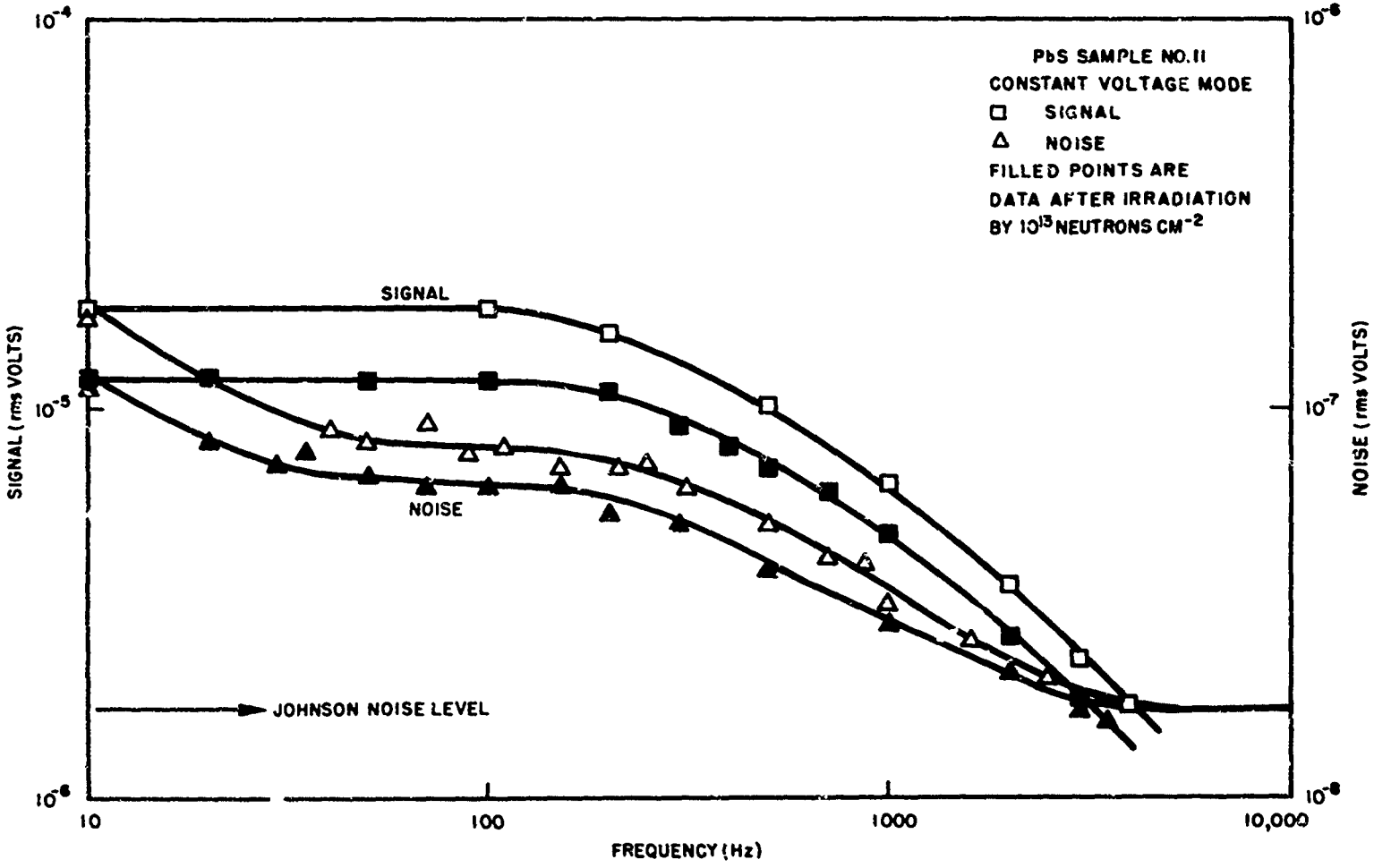

Fig. 9 - Frequency response of the signal and noise for PbS sample No. 11. Filled points were measured after exposure to 10^{13} neutrons/cm^2. The noise bandwidth was 1 Hz.

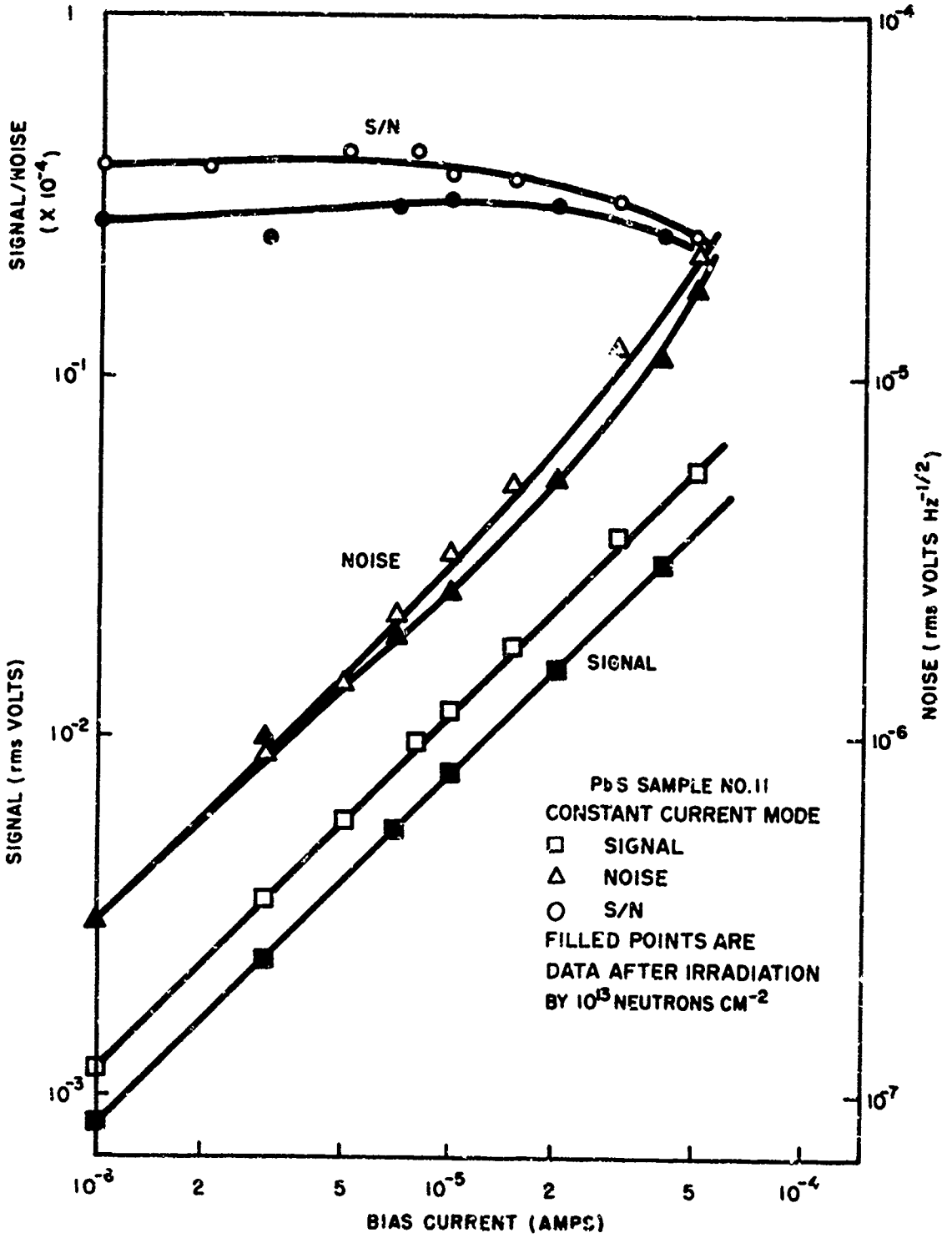

Fig. 10 - Signal, noise, and signal-to-noise ratio for sample No. 11. Filled points were measured after exposure to 10^{13} neutrons/cm^2.

(Page 20 is blank)

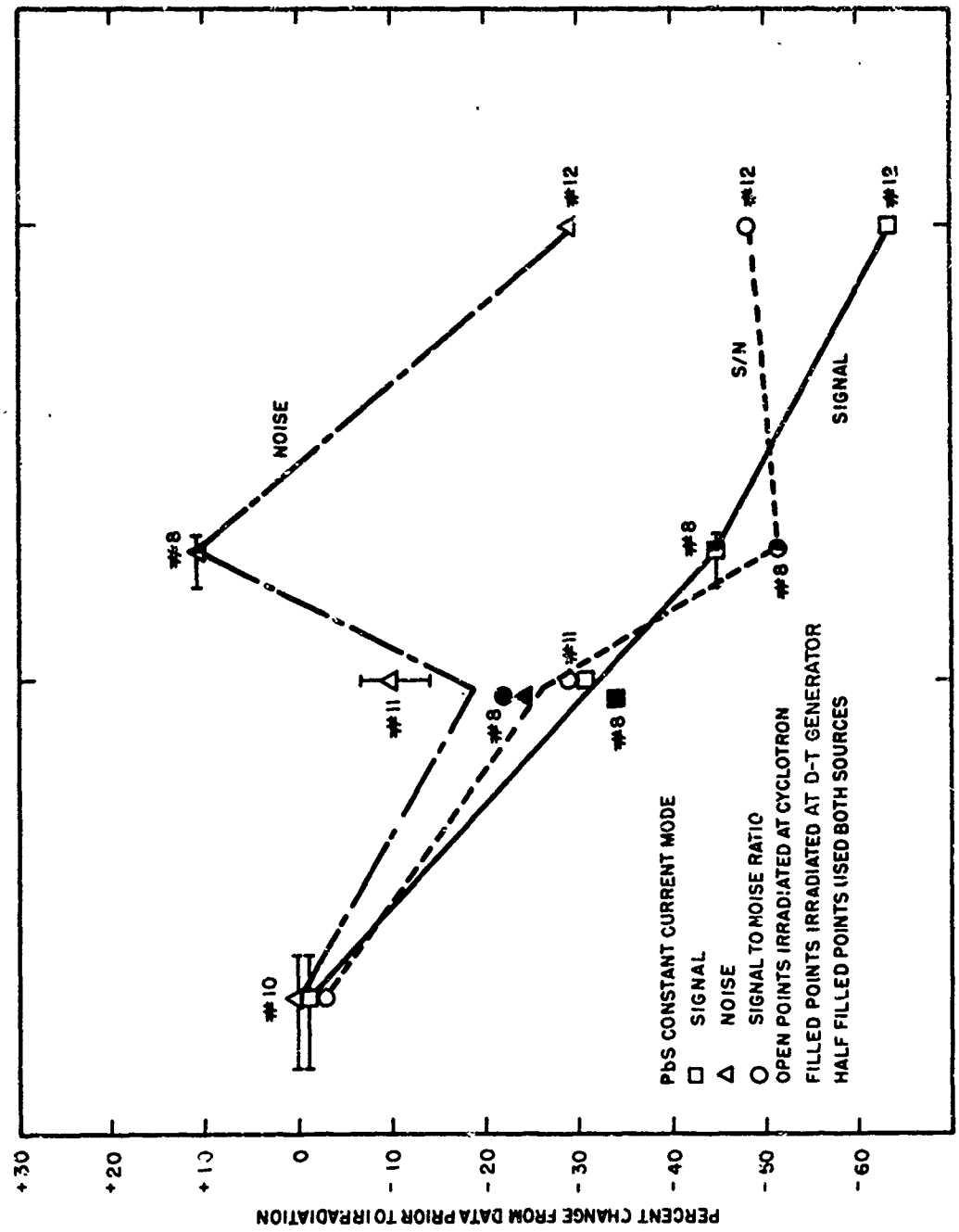

Fig. 11 – Change in signal, noise, and signal-to-noise after irradiation as a function of neutron fluence. Numbers next to the data points identify the detectors used.